Reaction products and their solidification process of the plasma sprayed Fe2O3–Al composite powders

ARTICLE *in* MATERIALS CHEMISTRY AND PHYSICS · MARCH 2012

Impact Factor: 2.26 · DOI: 10.1016/j.matchemphys.2012.01.006

7 AUTHORS, INCLUDING:

Dianran Yan
Hebei University of Technology
44 PUBLICATIONS **400** CITATIONS
SEE PROFILE

Yong Yang
32 PUBLICATIONS **283** CITATIONS
SEE PROFILE

Yanchun Dong
Hebei University of Technology
29 PUBLICATIONS **287** CITATIONS
SEE PROFILE

Materials Chemistry and Physics 133 (2012) 190–196

Contents lists available at SciVerse ScienceDirect

Materials Chemistry and Physics

journal homepage: www.elsevier.com/locate/matchemphys

Reaction products and their solidification process of the plasma sprayed Fe_2O_3–Al composite powders

Dianran Yan[a,b], Yong Yang[a,b,*], Yanchun Dong[a,b], Lei Wang[a,b], Xueguang Chen[a,b], Jianxin Zhang[a,b], Jining He[a,b]

[a] Key Lab. for New Type of Functional Materials in Hebei Province, Hebei University of Technology, Tianjin, China
[b] School of Materials Science and Engineering, Hebei University of Technology, Tianjin, China

ARTICLE INFO

Article history:
Received 5 June 2011
Received in revised form 4 December 2011
Accepted 1 January 2012

Keywords:
A. Composite materials
B. Coatings
Plasma spray
Thermite reaction

ABSTRACT

Fe_2O_3–Al composite powders were deposited onto steel substrate by plasma spraying. The reaction products of the Fe_2O_3–Al composite powders in the plasma flame and their solidification process were investigated. The results showed that the reaction products of the Fe_2O_3–Al composite powders in the plasma flame were Fe–Al–O ceramic melt and Fe melt. Fe was not always formed in the reaction products of each composite particle, and the formation of Fe was dependent on the composition distribution and the reaction kinetics process of each composite particle. The composition inhomogeneity, discontinuity and porousness of the composite particles resulted in the difference of the reaction kinetics of each composite particle and the composition difference of the droplets. Hercynite solid solution, Fe, Al_2O_3 and FeAl phases were formed by non-equilibrium solidification of the Fe–Al–O ceramic melt. For the smaller size droplet, when it spread on the substrate, the spreading droplet was quickly chilled to form equiaxed grains with size of 100–200 nm. Nano-sized or submicron equiaxed grains, nano-sized columnar grains and cellular structure were formed in the larger spreading droplet. Fe rich hercynite solid solution nucleated and grew preferentially and then Al rich hercynite solid solution grew, which form composition segregation in the columnar grains. The main phases in the composite coating were hercynite solid solution.

1. Introduction

The Fe_2O_3–Al mixture is a classical thermite system which has been used to produce alumina liners in situ inside pipes [1]. However, there were few reports about preparing coatings on the external surface of metals by the Fe_2O_3–Al thermite reaction system. The application of this reaction system was to prepare ceramic reinforced metal–matrix composites [2,3]. Combining the Fe_2O_3–Al thermite reaction with plasma spraying, the reaction process was controlled by changing spraying parameters, depositing speed and chilling level of reaction products on the surface of metal substrates. This was an efficient approach to prepare $FeAl_2O_4$ matrix composite coating on the external surface of metals [4]. The investigation results indicated that the crack extension force of the $FeAl_2O_4$ matrix composite coating prepared by plasma spraying Fe_2O_3–Al composite powders was 20% higher than that of the nanostructured Al_2O_3–3%TiO_2 coating and 100% higher than that of the microstructured Al_2O_3–3%TiO_2 coating [5]. The microstructure of the coating is dependent on the reaction products of thermite reaction system and the solidification process of the reaction products [6]. Therefore, it is significant to investigate the reaction products of Fe_2O_3–Al thermite reaction in the plasma flame and the solidification process of the reaction products.

The products of thermite reaction between Al and Fe_2O_3 in different processing conditions had been extensively studied [7–12]. It was indicated that the chemical composition and phases of the reaction products of the thermite reaction were mainly dependent on the reactants composition, reaction extent and cooling conditions. Reaction process and reaction products of Fe_2O_3–Al composite powders in plasma flame were different from the conventional Fe_2O_3–Al thermite system, due to the high temperature, high heating rate, short reaction time, high depositing velocity, high cooling rate, the composition inhomogeneity of Fe_2O_3–Al composite powders and the isolated reaction process for a composite particle. Further, the solidification process of the reaction products was also different from that of the conventional Fe_2O_3–Al thermite system. Therefore, the present investigation focused on the reaction products of Fe_2O_3–Al thermite system in the plasma flame and the solidification process of the reaction products.

* Corresponding author at: No. 29 Guangrong Road, Hongqiao District, Tianjin 300132, China. Tel.: +86 22 60204581; fax: +86 22 26564581.
E-mail addresses: yandianran@126.com (D. Yan), yangyong@hebut.edu.cn, yangyonghebut@163.com (Y. Yang).

0254-0584/$ – see front matter © 2012 Elsevier B.V. All rights reserved.
doi:10.1016/j.matchemphys.2012.01.006

Table 1
The main plasma spraying parameters.

	Voltage (V)	Current (A)	Primary gas (Ar) flow rate (L min^{-1})	Secondary gas (H_2) flow rate (L min^{-1})	Carrier gas flow rate	Torch nozzle		Spray distance (mm)
						Torch efficiency (kW)	Injector position	
Ni–Al coating	70	500	80	20	8	35	Radial, outside of the nozzle	80–100
Composite coating	60	500	80	20	8	30	Radial, outside of the nozzle	80–100

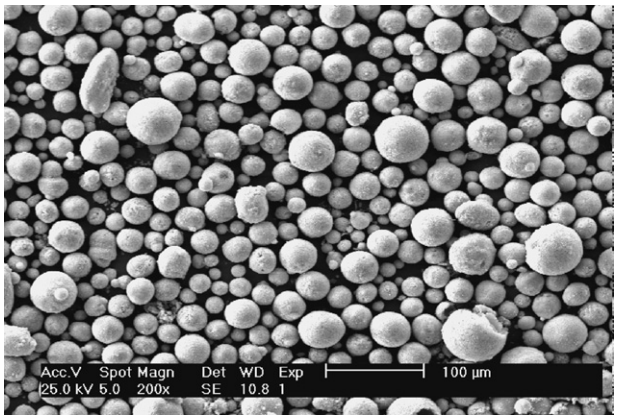

Fig. 1. SEM micrograph of the Fe_2O_3–Al composite powders.

2. Materials and methods

Fe–0.14–0.22wt%C steel was used as substrate which was machined into samples of 30 mm × 25 mm × 10 mm, and ground to obtain R_α > 25 μm rough surface. Fe_2O_3 and Al powders were used for spraying composite coating. The average particle size of Fe_2O_3 powder is about 0.6–0.8 μm (the Third Reagent Company of Tianjin, China). The average particle size of Al powder is 4–5 μm (Anshan Micropowder Limited Company, China). The powders were blended uniformly to produce a powder mixture with molar ratio composition of 1:2 of Fe_2O_3 and Al. The Fe_2O_3 and Al powders were blended uniformly to produce viscous slurry with the addition of binder (PVA) and deionized water. The slurry of powder mixture was spray dried to prepare composite powders by centrifugal spray dryer. The average particle size of the Fe_2O_3–Al composite powders is 30–60 μm (Fig. 1). The XRD pattern of the Fe_2O_3–Al composite powders is shown in Fig. 2. A bond coating of Ni–10 wt.%Al with thickness about 100 μm was deposited onto the substrate in order to increase the adhesive strength between the composite coating and the substrate. The as-prepared Fe_2O_3–Al composite powders were then plasma sprayed onto the bond coatings for about 300 μm in thickness, respectively. The coatings were plasma sprayed using GDP-2 type 50 kW plasma spraying device (Jiu Jiang Spraying Device Company, China). The spraying processing parameters are shown in Table 1. The temperature and velocity of the composite powders in the plasma flame were measured by the on-line measurement equipment Spray Watch 2i (Oseir Co., Ltd., Finland). The measurement volume of the in-flight particles characteristics was 23.72 mm × 29.62 mm × 6 mm. The phase constitution of the as-prepared coating was characterized by X-ray diffraction (XRD, Philips X'-Pert MPD) with Cu Kα radiation. A scanning electron microscope (SEM, Philips XL30/TMP) equipped with X-ray energy dispersive spectroscope (EDS) was employed to characterize the morphologies of the composite powders and the surface and cross-section of the coating.

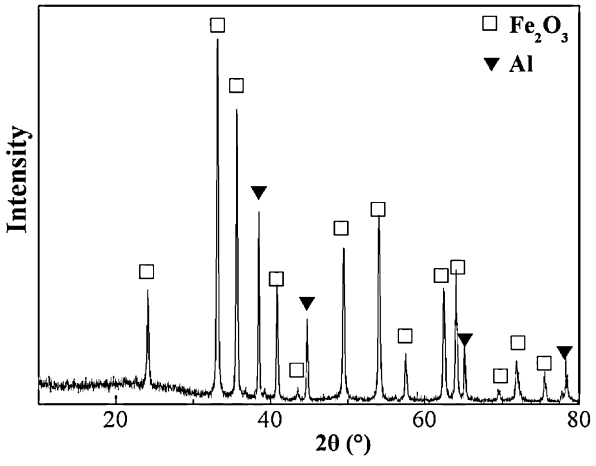

Fig. 2. XRD pattern of the Fe_2O_3–Al composite powders.

3. Results and discussion

3.1. Phase composition and microstructure of the composite coating

Fig. 3a shows the XRD pattern of the as-prepared coating. The diffraction peaks of $FeAl_2O_4$, Fe, Al_2O_3 and Fe–Al alloy were clearly indexed, and $FeAl_2O_4$ and Fe were the main phases in the coating. Fig. 3b shows the cross-section back-scattered SEM micrograph of the composite coating. It can be seen that the composite coating consisted of four kinds of different color regions, white particles (A region), wavy-like morphology black region (B region), gray region (C region) and light gray region (D region). The EDS analysis results of A, B, C and D regions are shown in Table 2. XRD, SEM and EDS results indicated that the matrix of the composite coating was hercynite solid solution ($xFeO{\cdot}yAl_2O_3$) with spinel structure. The color difference of the hercynite solid solution (H_{SS}) indicated there were different content of Al or Fe in the H_{SS}. The black region was rich in Al, and the gray region and light gray regions were rich in Fe.

The SEM micrographs of the surface of the composite coating after etched by 4 wt.% $FeCl_3$ solution for 100 min showed that there were two kinds of microstructure with different morphology in the composite coating (Figs. 4a and 6a). There were two kinds of morphologies (E and F) in Fig. 4a. E region was lightly etched, and F region was heavily etched. The high magnification of E region (Fig. 4b) showed that the composite coating consisted of white network structure and gray structure inside the network. The high

Table 2
EDS results of the composite coating corresponding to Fig. 3.

	Fe (at.%)	Al (at.%)	O (at.%)
A	89.56	4.71	5.73
B	12.99	31.33	55.68
C	17.11	30.23	52.66
D	32.29	17.17	50.54

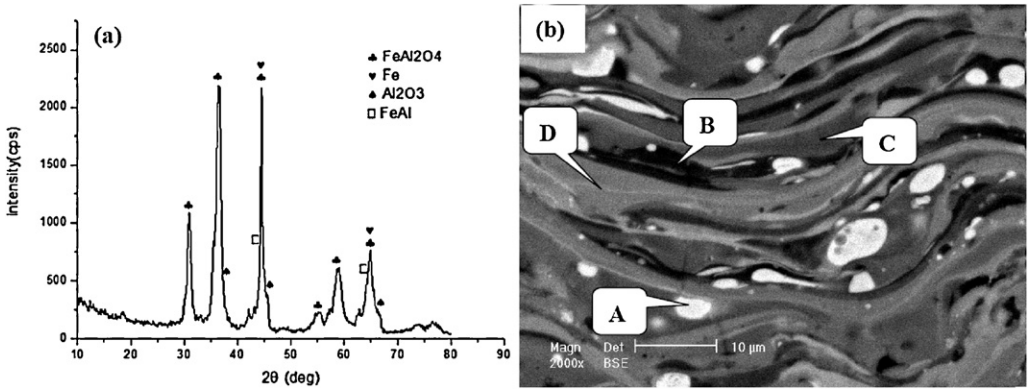

Fig. 3. XRD pattern (a) and cross-sectional back-scattered SEM micrograph (b) of the composite coating.

Table 3
EDS results of the composite coating corresponding to the G and H regions in Fig. 4b and c.

	Fe (at.%)	Al (at.%)	O (at.%)
G	26.88	19.00	54.12
H	17.19	26.15	56.66

magnification of F region (Fig. 4c) showed that the wall thickness of the network structure was 100–200 nm and the gray structure inside the network were etched off after long time etch. The EDS results of the white and gray structures in Table 3 show that the two kinds of structures were composed of Fe, Al and O. According to $FeO–Al_2O_3$ binary phase diagram and Fe–Al–O ternary phase diagram at 1000 °C [13], the hercynite was intermediate phase with fixed composition $FeAl_2O_4$ at low temperature. But the FeO and Al_2O_3 phases formed H_{SS} at high temperature, and H_{SS} had a wide range composition. It can be inferred that the network structure was H_{SS} dissolved with more Al_2O_3 and the structure inside the network was H_{SS} dissolved with more FeO.

Fig. 5 shows the cross-section SEM micrographs of the composite coating after etched by $FeCl_3$ solution. It can be seen from Fig. 5a that there were columnar grains structure (I region) in the sub-layer of the composite coating. The top of the sub-layer (J region) was harder to be etched than the interior of the sub-layer (I region), which indicated that the composition or structure of the top and the interior of the sub-layer was different. Fig. 5b shows that the columnar grains structure was etched into tubular structure, which corresponded to the microstructure in Fig. 4. It can be inferred from Figs. 4b and 5b that the microstructure in the sub-layer was cellular structure.

Fig. 6a shows that the other kind of microstructure in the composite coating. Fig. 6b is the high magnification of K region in Fig. 6a, showing the profile of the etch surface. Fig. 6c is the high

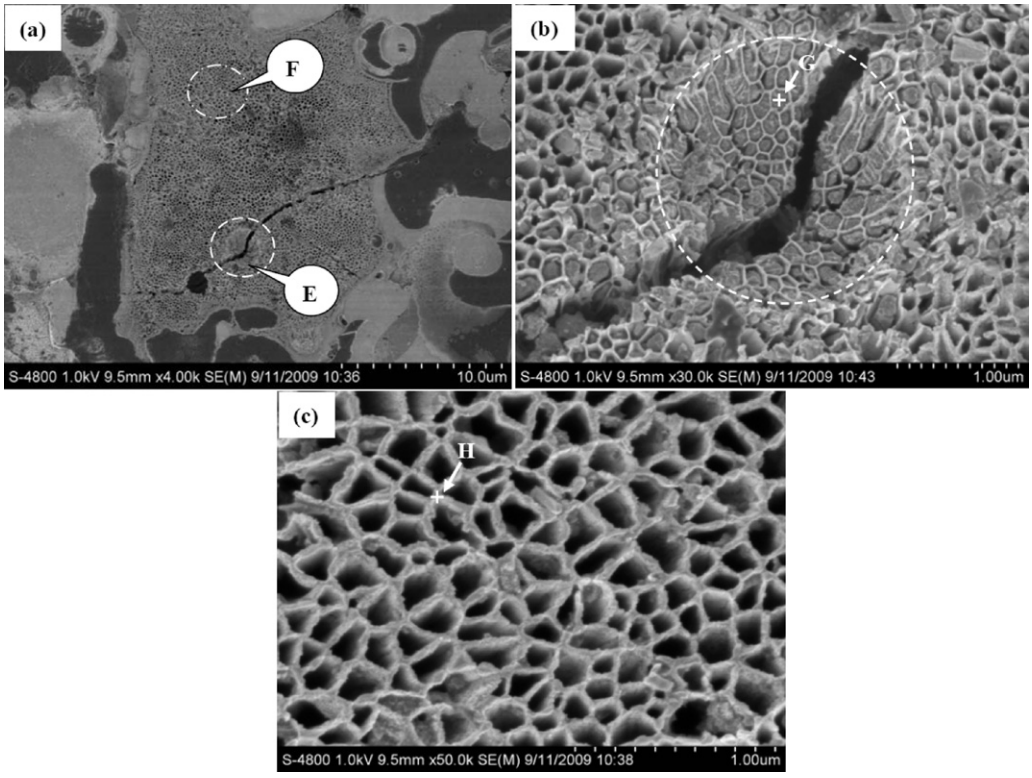

Fig. 4. SEM micrographs of the surface of the composite coating after etched by $FeCl_3$ (a), (b) high magnification of E region in (a) and (c) high magnification of F region in (a).

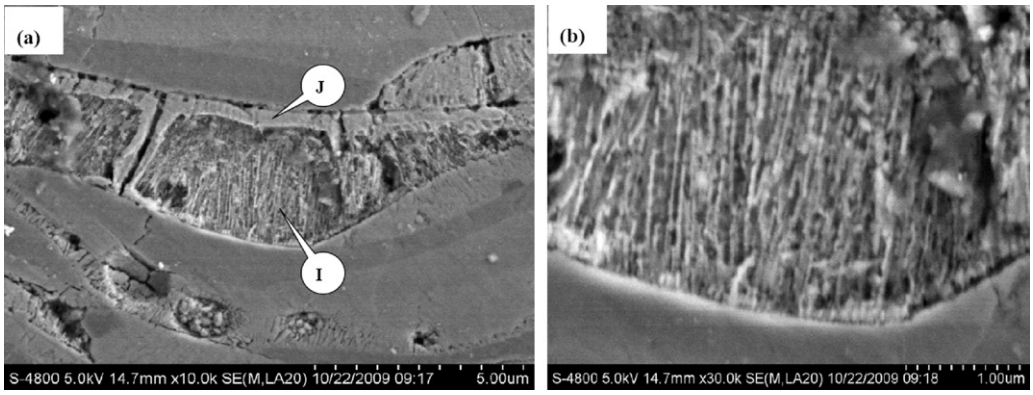

Fig. 5. Cross-section SEM micrographs of the composite coating after etched by $FeCl_3$ (a), (b) high magnification of "I" region in (a).

magnification of L region in Fig. 6a, showing the bottom of the etch surface. It can be seen from Fig. 6b that this kind of sub-layer in the composite coating was composed of single phase columnar grains. Fig. 6c shows that the diameters of the columnar grains were about 100–200 nm. The centers of most columnar grains were etched to form etch pits, which indicated that there was composition segregation in the columnar grains. The composition segregation in the columnar grains indicated that solidification of ceramic melt showed the characteristic of solid solution non-equilibrium solidification. The EDS result of the surface of the columnar grains (M region) was Fe 17.88 at.%, Al 26.62 at.% and O 55.50 at.%, which was similar to that of the network structure.

The above results showed that there were two kinds of microstructure with different morphology in the composite coating. One was cellular structure, and the other was columnar grains structure. And there was composition segregation in the columnar grains.

3.2. Reaction products and their solidification process of the Fe_2O_3–Al composite powders in the plasma flame

3.2.1. Temperature and velocity changes of the composite particles

Fig. 7 shows the temperature and velocity of the composite particles in the plasma flame vs. the spray distance. It can be seen from Fig. 7a that the particle temperature reached the maximum temperature 3274.5 °C at the spray distance of 100 mm, which was higher than that of the Al_2O_3 particles (2893 °C) in the plasma flame [14,15]. This indicated the composite powders had reacted in the plasma flame, and the reaction heat increased the temperature of the composite particles. The particle temperature then decreased with increasing of the spray distance, which indicated that the reaction between Fe_2O_3 and Al powders was completed at the spray distance of 100 mm. Fig. 7b shows the velocity of the composite particles in the plasma flame vs. the spray distance. Combined Fig. 7b

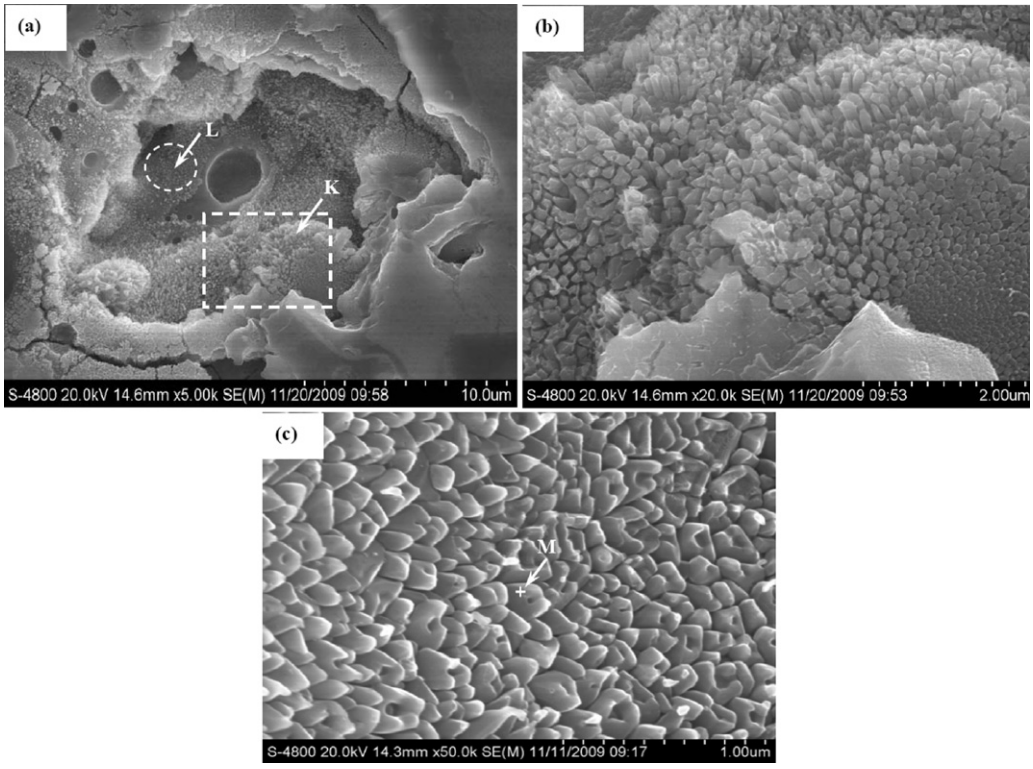

Fig. 6. SEM micrographs of the surface of the composite coating after etched by $FeCl_3$ (a), (b) high magnification of K region in (a) and (c) high magnification of L region in (a).

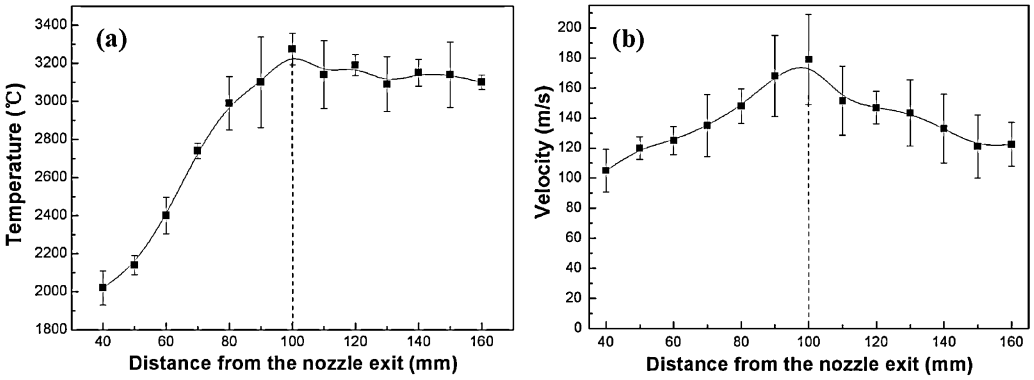

Fig. 7. The temperature and velocity of the composite particles in the plasma flame vs. the spray distance.

with Fig. 7a, it can be seen that when the reaction products reached the maximum temperature, the particles reached the maximum velocity (179 m s^{-1}), which was the same as the maximum velocity of the Al_2O_3–TiO_2 composite particles in the plasma flame [16,17]. That indicated the reaction of the composite particles did not affect their velocity in the plasma flame. The spray distance used in the coating preparing process was 100 mm, so the temperature and velocity of the particles before deposition on the substrate was 3274.5 °C and 179 m s^{-1}, respectively. It could be calculated that the staying time of the composite particles in plasma flame was only 0.5 ms.

3.2.2. Reaction products of the composite powders

Fig. 8 shows the SEM micrographs of the droplets morphology after deposition on the glass substrate, and Table 4 shows the EDS results of different regions in Fig. 8. It can be seen that the droplets were well spread on the glass substrate and the composition of the droplets included Fe, Al and O, which indicated that the droplets were Fe–Al–O melt before deposition. Table 4 shows that there was much composition difference in the different droplets (N and P). Most of the droplets were rich in Al (N), and a few droplets were rich in Fe (P). There were some white particles (Q and R) around the droplets rich in Al (N), and EDS results indicated that there were more Fe and a little Al and O in the particles (Q and R). It can be inferred from the XRD results (Fig. 3a) that these particles were Fe solid solution dissolving a little Al and O. However, there were no similar particles around the droplets rich in Fe (P), which indicated that Fe was not formed in the Fe_2O_3–Al thermite reaction of some composite particles and this was consistent with literature [8]. The region rich in Al and O were not detected in the deposition droplets, indicating that the single phase Al_2O_3 was not always formed in the reaction products of the composite powders. The above results indicated that the reaction kinetics of each composite particle in the plasma flame was different.

Fig. 8 indicates that the composition difference of each composite particle resulted in the difference of the reaction kinetics and the reaction products of each composite particle. The reaction products of the composite powders in the plasma flame had two kinds of state. One was the single Fe–Al–O ceramic melt, and the other was Fe–Al–O ceramic melt and Fe melt dissolving with Al and O. The $FeAl_2O_4$, Fe, Al_2O_3 and FeAl phases in the coating were the solidification products of Fe–Al–O ceramic melt and Fe melt.

Table 4
EDS results of different regions of the spreading droplets in Fig. 8.

	Fe (at.%)	Al (at.%)	O (at.%)
N	14.57	40.33	45.09
P	54.29	08.29	37.42
Q	78.72	10.39	10.88
R	72.96	13.05	13.99

The composition difference of the droplets was attributed to the composition inhomogeneity, discontinuity and porousness of the composite particles. The inhomogeneity of composite particles (Fe_2O_3 and Al powders) resulted in the difference of reaction products. If Fe_2O_3 was superabundant, the un-reacted Fe_2O_3 would decompose into FeO and O_2 [8], and then FeO would dissolve in Fe–Al–O ceramic melt. If Al was superabundant, the un-reacted Al would partly dissolve in the reaction products (for example Fe) or be partly gasified to form gaseous Al (the boiling temperature of Al is 2520 °C [7]) which may react with O_2 to form Al_2O_3, and then Al_2O_3 would be melted into Fe–Al–O ceramic melt at high temperature. Since Fe and the Fe–Al–O ceramic melt are not wetting, when there was Fe in the composite particle, Fe would exist as single liquid phase.

The above results indicated that after reaction of the composite powders, the reaction products, the intermediate phase and the superabundant Fe_2O_3 and Al were melted by the reaction heat to form Fe–Al–O ceramic melt. The composition inhomogeneity, discontinuity and porousness of the composite particles resulted in the difference of the reaction kinetics of each composite particle and the composition difference of the droplets.

3.2.3. Solidification process of the droplets

It can be seen from Fig. 1 that the composite particles were 7–40 μm. Experimental results showed that the volume shrinkage of the feedstock particles was about 16–20%, which was taken as 18%. The single droplet was, therefore, about 5.74–32.8 μm before deposition on the substrate. According to literature [18], the ratio of particle diameter to thickness of spread particle was (4–10):1, which was taken as 6:1. The thickness of spread particle was, therefore, about 1–5 μm, which was consistent with the layer thickness in Fig. 3b. The bottom of the droplet contacted with the substrate and the surface of the droplet contacted with the atmosphere after spreading on the substrate. Supposing that the temperature of the substrate was 200 °C (there was previously deposited layer), and the room temperature was 25 °C. For the larger size droplet, when it spread on the substrate, the chilling temperature of the surface of the spreading droplet was −3249 °C, and the undercooling temperature was 1755 °C. The chilling temperature of the bottom of the spreading droplet was −3074 °C, and the undercooling temperature was 1680 °C. The liquid in the bottom and surface of the spreading droplet were quickly chilled to form nanosized or submicron equiaxed grains. The cooling rate of the bottom decreased due to the temperature increasing of the substrate. The fastest cooling rate direction was perpendicular to the surface of the spreading droplet, and therefore, in the spreading droplet, negative

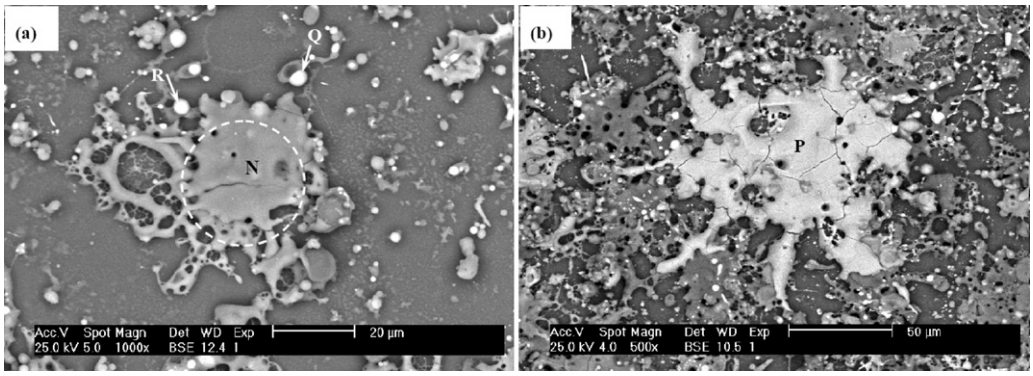

Fig. 8. SEM micrographs of the droplets morphology after deposition on the glass substrate.

temperature gradient was formed along the normal direction of the surface of the spreading droplet.

For the smaller size droplet, when it spread on the substrate, the spreading droplet was quickly chilled to form equiaxed grains with size of 100–200 nm, which was consistent with the TEM characterization results [19]. For the thicker size droplet with higher negative temperature gradient, the bottom and surface of the spreading droplet was chilled to form nano-sized or submicron equiaxed grains. The nano-sized or submicron equiaxed grains at the bottom preferentially grew to form nano-sized columnar grains. The solidification process of the spreading droplet was considered as non-equilibrium directional solidification of Fe–Al–O ceramic melt.

Table 4 indicates that the droplet had a wide range composition, which was consistent with the composition variation of H_{SS} described by the Fe–Al–O ternary phase diagram at 1000 °C. Hercynite rich in Fe nucleated and grew preferentially due to their favorable condition of the composition. The growth of the hercynite rich in Fe created favorable composition condition for the growth of the hercynite rich in Al. The center of the columnar grains grew as the hercynite rich in Fe, and the surface of the columnar grains grew as the hercynite rich in Al. That was the reason for the formation of the microstructure in Fig. 6. For the droplet rich in Al, if the composition of the Fe–Al–O melt reached the composition of $FeO–Al_2O_3$ eutectic in the growth process of the columnar grains, the melt would grew as divorced eutectic, and therefore form the cellular microstructure in Fig. 4b. The eutectic reaction did not progress completely due to the fast cooling rate, and therefore the composition of the wall of the cellular structure (network) was not the single phase Al_2O_3 but hercynite rich in Al.

4. Conclusion

In this paper, the reaction products of the Fe_2O_3–Al composite powders in the plasma flame and their solidification process were investigated. The results showed that:

(1) The reaction products of the Fe_2O_3–Al composite powders in the plasma flame were Fe–Al–O ceramic melt, and $FeAl_2O_4$, Fe, Al_2O_3 and FeAl phases were formed due to the non-equilibrium directional solidification of the Fe–Al–O ceramic melt.
(2) The composition inhomogeneity, discontinuity and porousness of the composite particles resulted in the difference of the reaction kinetics of each composite particle and the composition difference of the droplets.
(3) For the smaller size droplet, when it spread on the substrate, the spreading droplet was quickly chilled to form equiaxed grains with size of 100–200 nm. The solidification process of the larger size spreading droplet was considered as non-equilibrium directional solidification, and nano-sized or submicron equiaxed grains, nano-sized columnar grains and cellular microstructure were formed in the spreading droplet.
(4) Fe rich hercynite solid solution nucleated and grew preferentially, and then Al rich hercynite solid solution grew. The main phases in the composite coating were hercynite solid solution.
(5) Fe phase was not always present in the reaction products of the composite powders, and the formation of Fe was dependent on the composition distribution and the reaction kinetics process of each composite particle.

Acknowledgments

The authors gratefully acknowledge the financial supports of the National Natural Science Foundation of China (Grant Nos. 51072045 and 51102074), China Postdoctoral Science Foundation (Grant No. 20110490979) and the Natural Science Foundation of Heibei province, China (Grant No. 10965126D).

References

[1] J.J. Moore, H.J. Feng, Combustion synthesis of advanced materials. Part II. Classification and applications and modelling, Prog. Mater. Sci. 39 (1995) 275–316.
[2] N. Travitzky, P. Kumar, K.H. Sandhage, R. Janssen, N. Claussen, Rapid synthesis of Al_2O_3 reinforced Fe–Cr–Ni composites, Mater. Sci. Eng. A 344 (2003) 245–252.
[3] J. Umeda, M. Kawakami, K. Kondoh, E. Ayman, H. Imai, Microstructural and mechanical properties of titanium particulate reinforced magnesium composite materials, Mater. Chem. Phys. 123 (2010) 649–657.
[4] Y. Dong, D. Yan, J. He, X. Li, W. Feng, H. Liu, Studies on composite coatings prepared by plasma spraying Fe_2O_3–Al self-reaction composite powders, Surf. Coat. Technol. 179 (2004) 223–228.
[5] W. Tian, Y. Wang, T. Zhang, Y. Yang, Sliding wear and electrochemical corrosion behavior of plasma sprayed nanocomposite Al_2O_3–13%TiO_2 coatings, Mater. Chem. Phys. 118 (2009) 37–45.
[6] L.M. Wang, C.C. Chen, J.W. Yeh, S.T. Ke, The microstructure and strengthening mechanism of thermal spray coating $Ni_xCo_{0.6}Fe_{0.2}Cr_ySi_zAlTi_{0.2}$ high-entropy alloys, Mater. Chem. Phys. 126 (2011) 880–885.
[7] J. Mei, R.D. Halldearn, P. Xiao, Mechanisms of the aluminium-iron oxide thermite reaction, Scr. Mater. 41 (1999) 541–548.
[8] L. Duraes, B.F.O. Costa, R. Santos, A. Correia, J. Campos, A. Portugal, Fe_2O_3/aluminum thermite reaction intermediate and final products characterization, Mater. Sci. Eng. A 465 (2007) 199–210.
[9] P.M. Botta, R.C. Mercader, E.F. Aglietti, J.M. Porto Lopez, Synthesis of Fe–$FeAl_2O_4$–Al_2O_3 by high-energy ball milling of Al–Fe_3O_4 mixtures, Scr. Mater. 48 (2003) 1093–1098.
[10] C. Cuadrado-Laborde, L.C. Damonte, L. Mendoza-Zelis, L.M. Socolovsky, I.L. Torriani, Magnetic characterization of the mechanically induced thermite reaction between Fe_2O_3 and Al, Physica B 354 (2004) 125–128.
[11] G.F. Goya, H.R. Rechenberg, Mechanosynthesis of intermetallic $Fe_{100-x}Al_x$ obtained by reduction of Al/Fe_2O_3 composite, J. Phys.: Condens. Matter 12 (2000) 10579–10590.
[12] V.A. Shabashov, V.V. Sagaradze, A.V. Litvinov, A.G. Mukoseev, N.F. Vildanova, Mechanical synthesis in the iron oxide–metal system, Mater. Sci. Eng. A 392 (2005) 62–72.
[13] Y.M. Chiang, D. Birnie, W.D. Kingery, Physical Ceramics, John Wiley & Sons, New York, 1997.

[14] Fr.-W. Bach, K. Möhwald, T. Rothardt, Particle image velocimetry in thermal spraying, Mater. Sci. Eng. A 383 (2004) 146–152.
[15] H.B. Xiong, L.L. Zheng, L. Li, Melting and oxidation behavior of in-flight particles in plasma spray process, Int. J. Heat Mass Transfer 48 (2005) 5121–5133.
[16] S. Guessasma, G. Montavon, C. Coddet, Velocity and temperature distributions of alumina–titania in-flight particles in the atmospheric plasma spray process, Surf. Coat. Technol. 192 (2005) 70–76.
[17] G. Shanmugavelayutham, V. Selvarajan, T.K. Thiyagarajan, P.V.A. Padmanabhan, K.P. Sreekumar, R.U. Satpute, In-flight particle behaviour and its effect on co-spraying of alumina–titania, Curr. Appl. Phys. 6 (2006) 41–47.
[18] J.R. Davis, Handbook of Thermal Spray Technology, ASM International, Materials Park, OH, USA, 2004.
[19] Y. Yang, D. Yan, Y. Dong, L. Wang, X. Chen, J. Zhang, J. He, X. Li, In situ nanostructured ceramic matrix composite coating prepared by plasma spraying composite powders, J. Alloys Compd. 509 (2011) L90–L94.